Evolution of the electronic structure of the Cr/Au(001) interface

D. G. O'Neill and J. H. Weaver
Department of Chemical Engineering and Materials Science, University of Minnesota, Minneapolis, Minnesota 55455
(Received 7 August 1987)

The electronic structure of Au(001)-supported Cr thin films from 1 to 16 monolayers (ML) thick have been examined with angle-resolved photoemission. The evolution of the Cr electronic structure indicates layer-by-layer growth mode. For 1 ML coverage, *three* odd-symmetry states are observed at point $\bar{\Gamma}$ with binding energies of 4.5, 0.8, and 0.5 eV. These have $\bar{\Gamma}_3$ or $d_{x^2-y^2}$ symmetry (4.5- and 0.5-eV structures) and $\bar{\Gamma}_5$ or $d_{xz,yz}$ symmetry (0.8-eV structure). When a second layer of Cr is grown, a second odd-symmetry $d_{xz,yz}$-derived band appears between 1.1 and 1.3 eV, and it marks the development of periodicity normal to the surface. At 6 ML coverage, the Cr(001) $\bar{\Gamma}_5$ surface state appears. At 12 ML coverage, we observe the odd-symmetry Δ_2 band that produces the nesting electron and hole Fermi surfaces.

INTRODUCTION

The electronic structures of bimetallic interfaces are currently being studied by numerous investigators for many different reasons and applications.[1–15] Common to most of these studies is the desire to understand, from a fundamental perspective, the unique properties of the interface and the properties of layered or modulated materials. Studies of the electronic structure of noble and near-noble-metal overlayers on similar substrates have shown that the component of crystal momentum perpendicular to the surface, $k_\perp$, is not a quantum number for monolayer films but that the d bands show bulklike behavior by 5–6 monolayers.[2,16] Although the number of experimental studies that can be compared with calculated band structures is few, there has been reasonable agreement in band ordering and the shapes of the dispersion curves.[3]

Surface and thin-film magnetism have been the central focus for many experimental and theoretical studies of transition-metal overlayers on noble-metal substrates.[8–15] Spin-polarized slab calculations predict enormous magnetic moments with values of 3.7 Bohr magnetons (μ_B) for 1 monolayer (ML) Cr/Au(001) (Ref. 10) and $3.0\mu_B$ for 1 ML Fe/Ag(001).[11] These same calculations predict moments for the surfaces of bulk materials that are reduced to $2.49\mu_B$ for Cr(001) (Ref. 10) and $2.9\mu_B$ for Fe(001).[11] Significantly, these values should be compared with bulk values of $0.59\mu_B$ for antiferromagnetic Cr and $2.2\mu_B$ for ferromagnetic Fe. Recent results by Onellion *et al.*[3] for 1 ML Fe/Cu(100) reported reasonable agreement between their angle-resolved photoemission results and their calculated bands. Drube and Himpsel[8] compared inverse photoemission results for V/Ag(111) and Mg/Ag(111) with earlier studies for a Ag–15 at. % Mn random alloy[17] and assigned an emission feature 1.7 eV above E_F to minority-spin Mn d states. Jonker *et al.*[9] investigated the 1-ML Fe/Ag(100) system with spin-polarized angle-resolved photoemission and indicated the absence of a magnetic moment parallel to the Fe surface. The possibility of a magnetic moment perpendicular to the surface could not be ruled out, however, and was suggested by a recent calculation.[12] Electron-capture spectroscopy experiments by Rau *et al.*[13] have indicated that the Cr(001) surface is magnetically ordered 15° below the bulk Néel temperature, that Ni possesses local magnetic order at twice the Curie temperature, and that short-range magnetic order is nonzero and nearly constant between 200 and 640 K for V(001).

The magnetic properties of Cr surfaces and Cr thin films are particularly interesting because calculations predict[10] the existence of magnetic moments 5 times the value of bulk Cr. These large moments are produced by an exchange splitting of 2.9 eV which has been thought to stabilize a ferromagnetic surface on an antiferromagnetic material. Experimentally, angle-resolved photoemission experiments by Klebanoff *et al.*[14] reported an increased near-surface Néel temperature. Qualitatively, enhanced surface magnetism has been attributed to the reduced coordination of surface atoms. Two consequences of the reduced symmetry have been discussed. First, it has been suggested that the narrowing of surface bands would modify the density of states at E_F and change the effective spin polarization. Second, the surface spin polarization might be altered when reduced *s-d* hybridization modifies band dispersion near E_F and changes in the occupation of majority- and minority-spin bands might occur. Thin-film magnetism is further complicated by the possibility of an overlayer-substrate interaction, but the extent and effect of hybridization is not well understood.

In this paper, we discuss the evolution of the Cr/Au(001) electronic structure. For this system, preliminary investigations by Zajac *et al.*[18] showed that Cr adatoms occupy fourfold hollow sites and stabilize the (1×1) termination as an atomically sharp interface is formed. Our results will show the electronic structure of a Cr monolayer, a Cr bilayer, and the evolution of the bulk Cr

energy bands. In addition, we will show that Cr/Au *d-d* hybridization is significant and should be included in models of a bimetallic interface.

EXPERIMENTAL TECHNIQUE

Angle-resolved photoelectron spectroscopy (ARPES) experiments were performed at the University of Wisconsin Synchrotron Radiation Center (Stoughton, WI) using the Seya-Namioka monochromator and beamline. The spectral output of the beamline, $12 \leq h\nu \leq 32$ eV, was linearly polarized with the electric field vector in the surface plane. In our geometry it was parallel to the Au[100] direction. The experimental system included a Vacuum Sciences Workshop 45-mm–mean-radius hemispherical analyzer on a two-axis goniometer, four-grid optics for low-energy electron diffraction, and standard sample-preparation capabilities. The analyzer was operated at a pass energy of 10 eV. The acceptance cone of $\pm 1.5°$ provided an energy resolution of 200–250 meV and a momentum resolution of ~ 0.06 Å^{-1}. For comparison, the corner of the (001) surface Brillouin zone (SBZ), $\bar{M}$, corresponds to 1.54 Å^{-1}.

The Au(100) crystal was cleaned with Ar-ion sputtering followed by annealing to 550 °C to produce a well-ordered, reconstructed surface, as verified by low-energy electron diffraction (LEED) and photoemission. The surface normal was aligned to within 0.5° of the Au [001] direction. After the cleaning procedures, the operating pressure of the system was 1×10^{-10} Torr (base pressure $\sim 5 \times 10^{-11}$ Torr). During sublimation of Cr from a resistively heated Ta boat, the pressure rose to $\sim 2 \times 10^{-10}$ Torr. Film thicknesses were determined with a calibrated quartz oscillator. The photoemission spectra were normalized to the incident photon flux and were used to verify, by the logarithmic attenuation of the bulk Au *d* bands, the existence of a sharp Cr/Au interface and also to cross-check the thickness monitor. Our results showed that well-ordered Cr overlayers in registry with the Au(001) substrate could be obtained by annealing the interface at ~ 100–120 °C. Films less than about 2 ML thick could be annealed after deposition onto a room-temperature substrate. To obtain optimal ordering in thicker films, the substrate was held at the elevated temperature during deposition.

We have used three different collection geometries to investigate the electronic structure of the evolving Cr/Au(001) interface, termed normal-emission, odd-symmetry, and even-symmetry modes.[19] Each could be selected along any vertical plane of the crystal. The normal-emission mode detects odd-symmetry initial states because the photoelectron momentum **q** is detected in the Au [001] direction which is perpendicular to the vector potential, **A** in the Au [010] direction. In the off-normal odd-symmetry mode, photoelectrons are detected in the mirror plane defined by the Au [010] direction. Again, **q** is perpendicular to **A** to highlight emission from odd-symmetry initial states along $\bar{\Sigma}$. The off-normal even-symmetry mode detects photoelectrons in the mirror plane defined by the Au [100] direction and, since **q** is parallel to **A**, even states along $\bar{\Sigma}$ are detected. Since we will discuss wave functions in terms of atomic orbitals, we will use the convention that z is in the Au [001] direction which is perpendicular to the surface and x (y) is in the surface plane and parallel to the Au [100] (Au [010]) direction.

RESULTS AND DISCUSSION

Normal-emission spectra for Cr coverages from 0 to 16 ML are shown in Fig. 1 to summarize the evolving structure of Cr. For thin films where $k_\perp$ is not a valid number, the collection geometry of normal emission with *s*-polarized radiation probes states at the surface Brillouin-zone center, $\bar{\Gamma}$, for all photon energies. In thick films where $k_\perp$ is a valid quantum number, it is possible to examine states in the bulk Brillouin zone along Γ-Δ-X for an fcc crystal, or along Γ-Δ-H for a bcc crystal, by changing photon energies. We will use the convention that barred symbols such as $\bar{\Gamma}$, $\bar{\Sigma}$, and $\bar{M}$ refer to points in the two-dimensional surface Brillouin zone (SBZ) while symbols without bars refer to points in the bulk Brillouin zone. For all of the energy-distribution curves (EDC's) in Fig. 1, emission from the Au substrate extends from ~ 2 to ~ 7 eV binding energy. Cr contributions appear from ~ 2 eV to E_F and near 4.5 eV. For Cr coverages below 4 ML, changes in the spectra reflect the evolution of the bulk Cr $d_{xz,yz}$-derived Δ_5 band (near E_F and marked by tic marks). Above 4 ML, emission near E_F is dominated

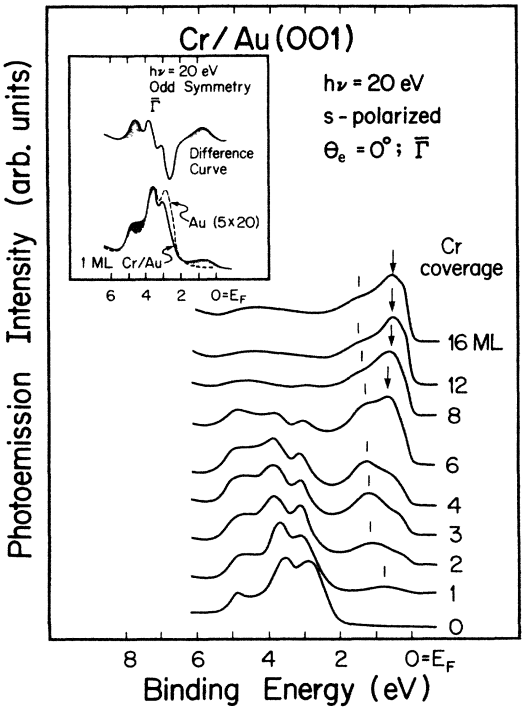

FIG. 1. Normal-emission spectra for Cr coverages from 0 to 16 ML Cr. The vertical bars highlight the evolution of the Δ_5 or $d_{xz,yz}$-derived bulk Cr band and the arrow points to the Cr $\bar{\Gamma}_5$ surface state which appears at 6 ML Cr coverage. The inset compares the spectra for clean Au(001) with 1 ML Cr/Au(001). Shading highlights the Cr-induced increases in intensity.

by a $\bar{\Gamma}_5$ surface state (arrows). To emphasize the intensity that is produced by a monolayer of Cr, we superimpose in the inset the spectra from clean Au and from 1 ML Cr/Au(001). The upper curve shows the difference between these two spectra. The shaded positive excursions highlight additions by Cr and negative excursions represent intensity losses.

The first Cr layer grows in two-dimensional patches which convert the (5×20) reconstructed Au layer to the (1×1) termination. This is illustrated in the left-hand panel of Fig. 2 where off-normal-emission EDC's reveal that the Au (5×20) surface-state emission at 1.8 eV diminishes as a function of increasing Cr coverage. EDC's on the right show the growth of Au (1×1) surface-state emission as the (5×20) surface is converted to the (1×1) surface. The onset of the increase in binding energy for the (1×1) surface state marks the completion of the first Cr layer and the development of the second layer (not shown). As discussed elsewhere,[5] the 0.7-eV energy shift is attributed to the conversion of the surface state into an interface state. Ultimately, this novel surface-interface state is lost through mixing with bulk Au states. Second-layer atoms also cause the Cr-induced intensity near 0.8 eV observed in normal emission (Fig. 1) to move to greater binding energy as new structure develops at 1.1 eV. Our results and those of others indicate that the overlayer growth is nearly ideal layer by layer.

Cr monolayer

The results of odd-symmetry off-normal measurements along the $\bar{\Sigma}$ symmetry line for the 1-ML Cr/Au(001) system are presented in Fig. 3. The left-hand panel shows the spectra between E_F and 9 eV, while the right-hand panel emphasizes Cr features near the Fermi level. Again, emission from the Au substrate extends from 2 to 7 eV while Cr contributions appear from 2 eV to E_F and near 4.5 eV. Emission from the Au(001)-(1×1) $\bar{M}_3$ surface state is observed on the left for $45°\leq\theta_e\leq60°$, where θ_e is the angle between the sample normal and the emitted photoelectrons.

The Cr-derived intensity near 4.5 eV (labeled A on the left) could only be identified at certain points along $\bar{\Sigma}$ because of the overlapping substrate emission. Therefore, we will concentrate on Cr emission near E_F and determine the symmetry and dispersion of the initial states responsible for this feature. There is one broad peak at ~0.7 eV for $\theta_e=0°$, which samples initial states at $\bar{\Gamma}$, while two features labeled B and C are separated by about 0.4 eV and are visible between $\theta_e=20°$ and 30°. At $\theta_e=50°$, which corresponds to $k_\parallel\sim1.52$ Å^{-1}, one peak is again observed at 0.55 eV binding energy. Spectra taken in the even-symmetry mode exhibit a single structure at 0.8 eV binding energy along $\bar{\Sigma}$, as shown by the dashed curve at $\theta_e=30°$ in Fig. 3.

The difference curve shown in the inset of Fig. 1 provides evidence for Cr/Au d-d hybridization. The large negative excursion represents a loss of intensity in the Au d bands that is produced by the presence of Cr adatoms. A similar feature is observed in a difference curve that is constructed from spectra for 1 ML Cr/Au(001) and the metastable Au(001)-(1×1) surface. The loss of intensity in the Au d bands is proved by rehybridization of surface layer d bands with the d states of the Cr monolayer. In-

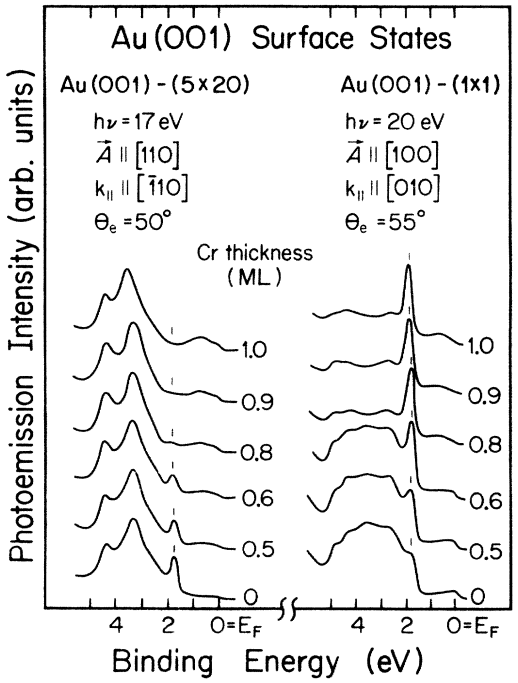

FIG. 2. Off-normal emission spectra showing the loss of the Au(001)-(5×20) surface state, left, and the growth of the Au(001)-(1×1) surface state, right, for submonolayer Cr coverages.

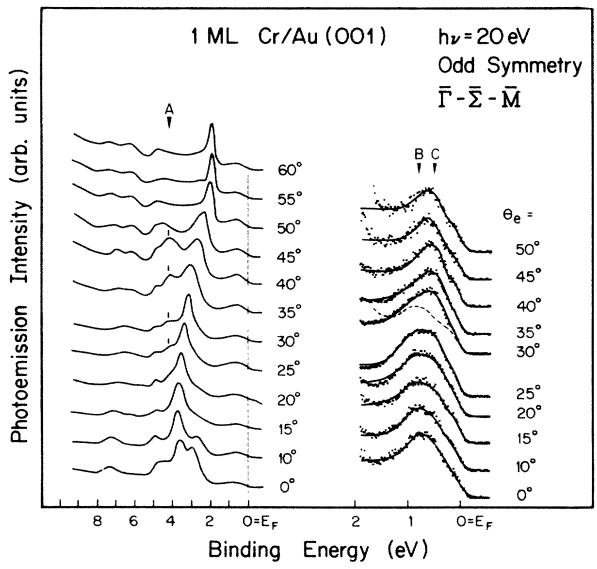

FIG. 3. Off-normal ARPES spectra for 1 ML Cr/Au(001). Emission from three Cr-derived odd-symmetry bands is observed along $\bar{\Sigma}$ at 4.5, 0.8, and 0.5 eV, labeled A, B, and C, respectively. The raw data shown as dots were obtained in the odd-symmetry collection mode and the solid lines are fits to the spectra, as described in the Appendix. The dashed curve was obtained in the even-symmetry mode.

termetallic d-band hybridization has been reported by Houston *et al.*[4] to explain a spectral feature that is unique to the 1-ML Cu/Ru(0001) interface. Although we do not observe a Cr/Au hybrid state, the difference curve in Fig. 1 is in agreement with the existence of intermetallic hybridization, as suggested for the Cu/Ru(0001) systems. Indeed, mixing of Au-derived and Cr-derived $d_{x^2-y^2}$ states is inevitable as they are degenerate over a portion of the Brillouin zone.[20] The effects of the hybridization will be discussed later in terms of the monolayer Cr-band structure.

The broad spectral intensities and relatively small band separation of the Cr-derived states preclude determination of the band structure by simple visual inspection. Peak deconvolution procedures were employed to obtain the necessary quantitative information, as discussed in the Appendix. The solid lines in Fig. 3 are calculated from this analysis and represent the best fit to the experimental odd-symmetry spectra. From that analysis, it is possible to determine the experimental band structure, E versus $k_{\parallel}$, shown in Fig. 4. The $\times$'s represent odd-symmetry states and the $+$'s represent even-symmetry states. To summarize, we detect four bands along $\bar{\Gamma}$-$\bar{\Sigma}$-$\bar{M}$ that are in the energy range from -0.5 to -4.5 eV, three of odd symmetry and one of even symmetry.

Each of the experimental bands in Fig. 4 can be identified with a particular wave function by using an analysis based on group theory and matrix-element effects. The appropriate symmetry group for the 1-ML Cr/Au(001) surface is the fourfold-symmetric C_{4v} group. Character tables for this group show two representations that are odd with respect to reflection about a vertical mirror plane.[21] There is one singly degenerate $\bar{\Gamma}_3$ representation which transforms as x^2-y^2 and a doubly degenerate $\bar{\Gamma}_5$ representation which transforms as xz,yz. Since the zone center and corner, $\bar{\Gamma}$ and $\bar{M}$, possess the full symmetry of the surface, we expect the $\bar{\Gamma}_3$ and $\bar{\Gamma}_5$ representations to be seen as $d_{x^2-y^2}$ and $d_{xz,yz}$ states, respectively. In contrast, states along $\bar{\Delta}$ and $\bar{\Sigma}$ do not possess the full C_{4v} symmetry of the surface but belong to the C_{2v} group representation. Correlation tables show that the twofold-degenerate xz,yz representation in the C_{4v} group (at $\bar{\Gamma}$) will split into two singly degenerate odd and even representations in the C_{2v} group (along $\bar{\Sigma}$). Additional information about the initial-state wave functions can be extracted through an analysis based on matrix-element effects. With light that is polarized in the xy plane (s polarized), the photoemission intensity from a $d_{x^2-y^2}$-derived wave function is proportional to $\sin^2\theta_e$, and such a state will have a very low intensity at normal emission but will increase in intensity as the exit angle is increased.

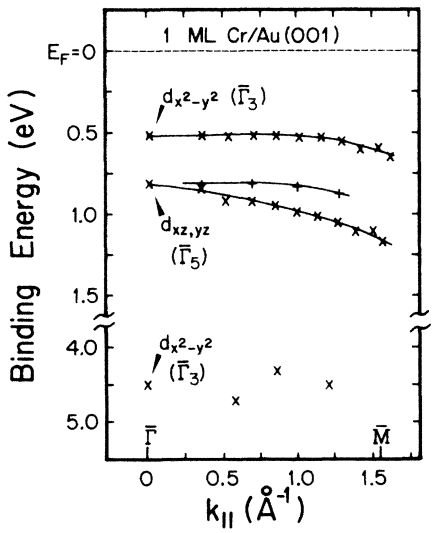

FIG. 4. Experimental plots of E vs $k_{\parallel}$(Å^{-1}) for 1 ML Cr/Au(001). The $\times$'s represent odd-symmetry states and $+$'s represent even-symmetry states. The existence of two $d_{x^2-y^2}$-derived bands at 4.5 and 0.5 eV can be explained by identifying the bands with majority- and minority-spin states, respectively, as discussed in the text.

With this analysis, each experimental band can be associated with emission from a specific initial-state wave function. The band with 0.8 eV binding energy at $\bar{\Gamma}$ has $d_{xz,yz}$ character since this state splits along $\bar{\Sigma}$ into an odd and an even band. The remaining two odd-symmetry features do not exhibit this behavior but, instead, increase in intensity as the exit angle is increased. The uppermost $d_{x^2-y^2}$ band at 0.5 eV has a sixfold increase in the intensity for exit angles between 0° and 40°. An increase is also observed in the 4.5-eV band, but the spectral overlap with the Au substrate precludes quantitative characterization. These two features exhibit behavior characteristic of emission from $d_{x^2-y^2}$-derived wave functions.

In band calculations for bimetallic interfaces, current theories model the substrate as a five- to nine-layer slab that is infinite in two dimensions and simulate the interface by adding layers of atoms on either side of the slab to maintain inversion symmetry. For transition metals, these calculations require a spin-dependent potential, the form of which is the subject of considerable theoretical effort. In Fig. 5, we show calculated spin-polarized E-versus-$k_{\parallel}$ curves from Fu and Freeman[22] based on their full-potential linear augmented-plane-wave (FLAPW) method. Solid lines reflect states that are at least 70% localized in the Cr monolayer. These results predict that the exchange splitting is $\sim$2.9 eV, producing separate energy regions for the majority- and minority-spin electrons. The magnitude of the splitting and the location of E_F between the two regions combine to produce a large spin polarization and the enhanced magnetic moments.[10,11] If an exchange splitting of $\sim$2.9 eV exists, as predicted by the FLAPW bands of Fig. 5, then emission from these states should be resolved using conventional (non-spin-resolved) techniques. This is true if either the surface Néel temperature, T_N, is above room temperature (the measurements were done at room temperature) or the exchange splitting is nonzero at or above T_N. For bulk Cr, T_N is 312 K.

The results summarized by the experimental band structure of Fig. 4 show the dispersion of three bands for 1 ML Cr/Au(001). The dispersion of the lower $d_{x^2-y^2}$-derived band was masked by substrate emission. Al-

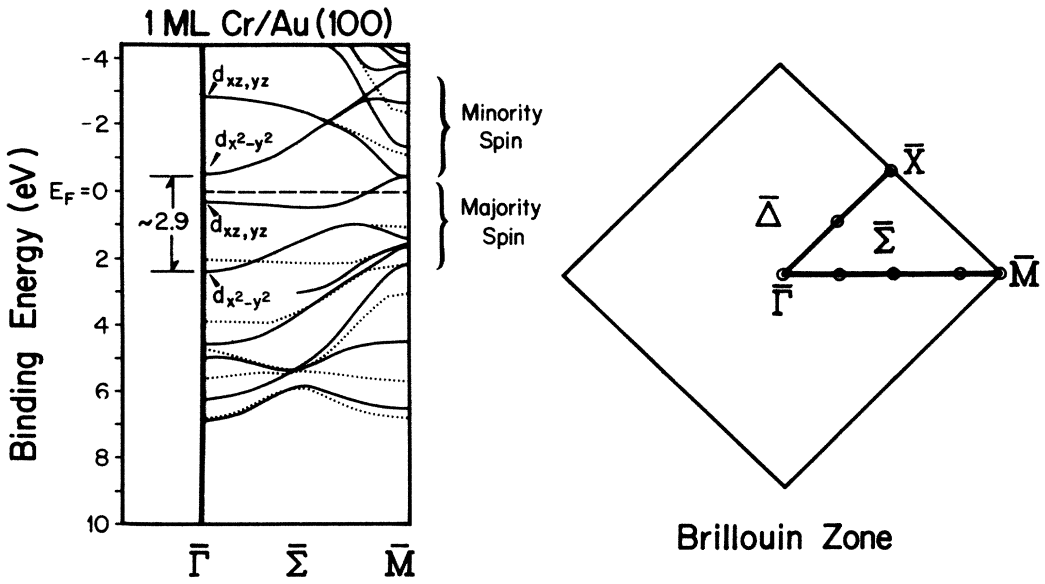

FIG. 5. Calculated bands for 1 ML Cr/Au(001) from Fu and Freeman (Ref. 20). The majority- and minority-spin bands are indicated with curly braces. The vertical bar highlights the calculated energy separation, 2.9 eV, between majority- and minority-spin $d_{x^2-y^2}$-derived states at $\bar{\Gamma}$. The right-hand panel shows the square surface Brillouin zone. The off-normal spectra presented in this paper detect states along $\bar{\Gamma}$-$\bar{\Sigma}$-$\bar{M}$.

though the calculations of Fig. 5 predict a distinctive minimum in the energy separation between the calculated $d_{x^2-y^2}$-derived and $d_{xz,yz}$-derived bands along $\bar{\Gamma}$-$\bar{\Sigma}$-$\bar{M}$, the experimental bands are less dispersive. As shown, the $d_{xz,yz}$-derived band moves from 0.7 to 1.2 eV and the $d_{x^2-y^2}$ band near 0.5 eV is even flatter in **k** space. The calculations predict an energy separation, between the majority-spin $d_{x^2-y^2}$ and $d_{xz,yz}$ states at $\bar{\Gamma}$, to be 2.1 eV. There are two experimental energy separations that could be compared to the predicted value. One is 3.7 eV and corresponds to the difference between the lower $d_{x^2-y^2}(\bar{\Gamma}_3)$ state and the $d_{xz,yz}(\bar{\Gamma}_5)$ state. The second is 0.3 eV and is the difference between the $\bar{\Gamma}_5$ and the upper $\bar{\Gamma}_3$ states. Since the lower $\bar{\Gamma}_3$ band eventually develops into the bulk $d_{x^2-y^2}$ band, we conclude that the relevant separation is 3.7 eV. The difference between theory and experiment is then intriguing, and may be due in part to Cr/Au *d-d* hybridization. (Evidence for Cr/Au *d-d* bonding was found in the difference spectra of Fig. 1.) This would increase the binding energy of the Cr $d_{x^2-y^2}$ states relative to the $d_{xz,yz}$ states.

In this comparison, we have associated the lower $d_{x^2-y^2}$-derived experimental band near 4.5 eV with majority-spin electrons. Similarly, the $d_{xz,yz}$-derived band at 0.8 eV was associated with majority-spin electrons. Although our spectra are not spin polarized and we are not measuring spin directly, the existence of majority and minority bands is implied by the existence of the three odd-symmetry states at $\bar{\Gamma}$. In particular, since the fourfold-symmetric Cr(001) surface has C_{4v} symmetry, there should be two different odd states at $\bar{\Gamma}$.[21] We find *three* odd states, and two of these have $d_{x^2-y^2}$ character. Since the splitting of the $d_{x^2-y^2}$ or $\bar{\Gamma}_3$ states is ~4 eV, we suggest that the $d_{x^2-y^2}$-derived emission at 0.5 eV reflects the minority-spin $\bar{\Gamma}_3$ state. This would give an exchange splitting of ~4 eV for a Cr(001) monolayer, a value which is consistent with the values predicted recently. At the same time, this is a tentative identification since we are not spin sensitive and its confirmation must await experimental studies using spin-polarized techniques.

Cr bilayer

In Fig. 6 we show the results of our odd-symmetry off-normal measurements along the $\bar{\Sigma}$ symmetry line for 2 ML Cr/Au(001). Comparison with the spectra of Fig. 3 shows that there is a peak shift from about −0.8 eV for the Cr monolayer to about −1.1 eV for the Cr bilayer. Difference curves reveal that the energy shift results from a new spectral feature with binding energy between −1.1 and −1.3 eV along $\bar{\Sigma}$. In Fig. 7 we show the experimental band structure for the Cr bilayer obtained from the results of Fig. 6. Two $d_{xz,yz}$-derived bands are observed along $\bar{\Sigma}$, where only one band was observed for the monolayer. It is important to note that the results for the Cr bilayer cannot be described as a superposition of the Cr monolayer bands and the new $d_{xz,yz}$-derived band. The upper $d_{xz,yz}$-derived band at 0.82 eV at $\bar{\Gamma}$ disperses to greater binding energy, but midway along $\bar{\Sigma}$ reverses direction and moves toward E_F as it approaches $\bar{M}$. The minority-spin $d_{x^2-y^2}$-derived band is modified as it now disperses toward E_F, reaching 0.4 eV binding energy near $\bar{M}$.

The interesting work of Ohnishi *et al.*,[23] which examined the evolution of the W(001) surface electronic struc-

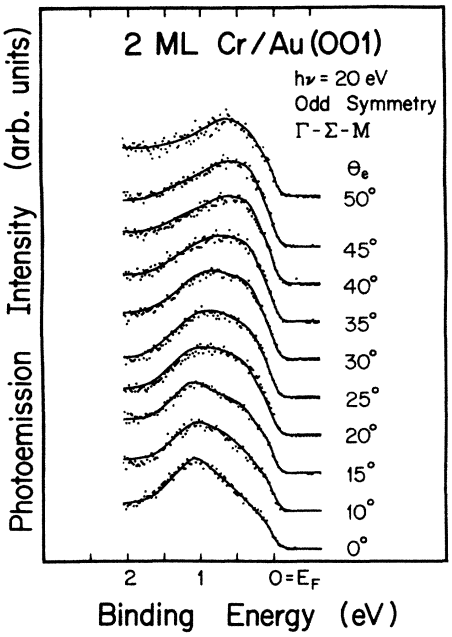

FIG. 6. Off-normal odd-symmetry photoemission spectra for 2 ML Cr/Au(001) analogous to those of Fig. 3 showing a shift in peak intensity from 0.8 to 1.1 eV.

ture, along with the work of Fu and Freeman which examined the Fe/Cu(001) interface,[6] makes it possible to compare our Cr/Au(001) experimental observations with the predictions of FLAPW calculations. If we compare the theoretical bands for an isolated W(001) monolayer with the bands from a three-layer slab, we see a trend which is similar to our experimental results. In particular, the W(001) monolayer has a single $d_{xz,yz}$-derived band that disperses from 1.4 eV above E_F to 0.4 eV below E_F,

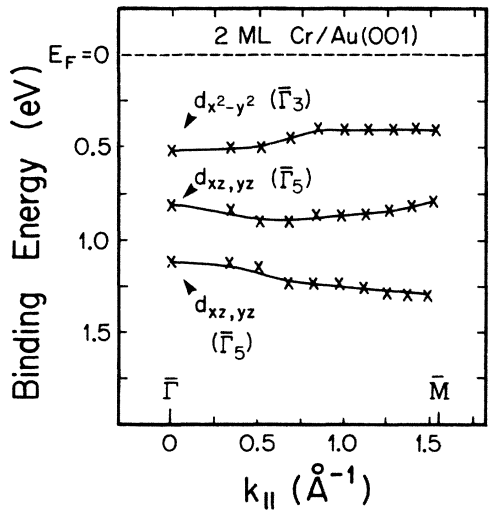

FIG. 7. Odd-symmetry experimental E-vs-$k_{\|}$ curves for 2 ML Cr/Au(001) from the results of Fig. 6. Two $d_{xz,yz}$-derived bands exist along $\bar{\Gamma}$-$\bar{\Sigma}$-$\bar{M}$ while 1 ML Cr/Au(001) has only one.

while two different $d_{xz,yz}$-derived bands are predicted for the three-layer slab. The theoretical majority-spin $d_{xz,yz}$-derived levels for 1 and 2 ML Fe/Cu(001) show the same trends.[6]

The two $\bar{\Gamma}_5$ or $d_{xz,yz}$ states in the Cr bilayer are precursors to the bulk Cr Δ_5 ($d_{xz,yz}$-derived) band that extends from about 1 eV below E_F at Γ to $\sim$1.3 eV above the Fermi level at $H_{25'}$.[24] Unfortunately, the width of these features precludes observation of states added by third, fourth, and subsequent layers.

Multilayer Cr films

The Cr electronic structure continues to change as the film thickness is increased from 2 to 12 ML. The third Cr layer produces a feature at the Fermi level in off-normal odd-symmetry spectra near the $\bar{M}$ point of the SBZ, $h\nu=20$ eV and $\theta_e=55°$ (see Fig. 1 of Ref. 5). This feature has negligible intensity for 2 ML Cr/Au(001) and grows with the third Cr layer. This suggests that the third layer forms after the second layer is nearly complete.

The first appearance of the Cr $\bar{\Gamma}$ surface state occurs at a coverage of 6 ML where it has a binding energy of 0.45

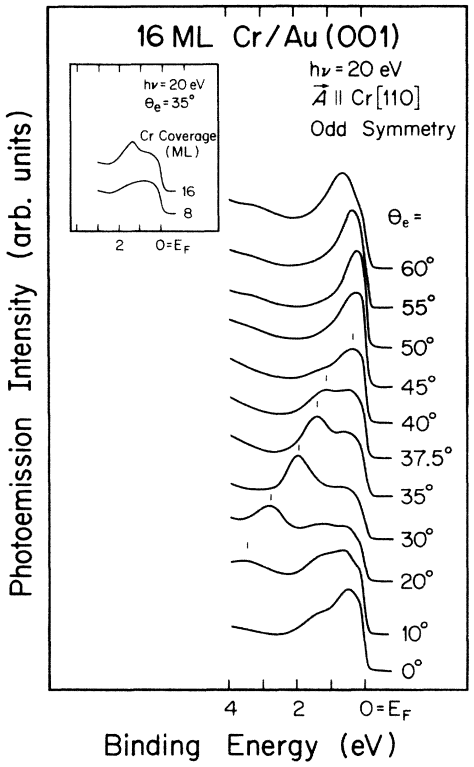

FIG. 8. Off-normal odd-symmetry spectra from the Cr(110) mirror plane for 16 ML Cr/Au(100). A dispersive Δ_2 odd-symmetry band is observed between 4 eV and E_F for $0\leq\theta_e\leq40°$. The states in this band near E_F stabilize the spin-density wave that is responsible for bulk Cr antiferromagnetic behavior, and these results indicate that 16-ML films are bulk-like. The inset compares spectra for 8 and 16 ML Cr for $\theta=35°$ to show that emission from the Δ_2 band appears only after 8 ML of Cr.

eV, as indicated by an arrow of Fig. 1. This feature is verified to be a surface state by its dispersion with $k_{\parallel}$, its lack of dispersion with $k_{\perp}$, and the ease with which it is quenched by 1 L CO (1 L = 1 langmuir $=10^{-6}$ torr sec). The location and existence of this surface state are in agreement with previous investigations of the Cr(001) surface.[14,24] Its appearance at 6 ML is also additional evidence for layer-by-layer overlayer growth. It is important to note that these results were obtained with fully annealed films and quite different results can be expected with unannealed films where a less than ideal layer-by-layer growth mode might be observed.

Finally, at 16 ML coverage, a very dispersive band is observed in off-normal odd-symmetry emission, as shown in Fig. 8. This Δ_2-symmetry band is not observed for 8 ML Cr/Au(001), as seen in the inset of Fig. 8. The electronic structure of bulk Cr has been studied by Gewinner *et al.*[24] using normal and off-normal emission from the Cr(100) surface. The experimental bands they obtained are in reasonable agreement with the calculated paramagnetic electronic structure of Asano and Yamashita.[25] In accord with their interpretation, the feature that we observed for θ_e between 0° and 40° is produced by emission from $d_{x^2-y^2}$-derived states along G, from H_{12} to N_4. The peak in the 50° and 60° spectra is produced by emission from $d_{xz,yz}$-derived states along D, near the P_4 point. For the antiferromagnetic (AFM) Brillouin zone, this interpretation would correspond to emission from states along Σ and T, respectively.[26]

The evolution of the magnetic properties from the monolayer to the thick coverages can be summarized through changes in the electronic structure. Previous studies have shown that the Δ_2 band, which is responsible for the dispersive feature in Fig. 8, is critical to antiferromagnetic behavior in Cr because these states form the nesting electron and hole Fermi surfaces that stabilize the AFM spin-density wave.[27] Therefore, the spectra in Fig. 8 suggest that bulklike magnetism requires a film thickness of at least 12 monolayers.

ACKNOWLEDGMENTS

We would like to thank the staff of the University of Wisconsin Synchrotron Radiation Center and the Physical Sciences Laboratory (Stoughton, WI) for providing a hospitable and stimulating environment in which to work. Discussions with A. J. Freeman, C. L. Fu, E. Wimmer, J. G. Gay, R. Richter, J. Tobin, and D. Huber were invaluable. A. J. Freeman and C. L. Fu generously provided the results of their calculations prior to publication. This work was supported by the National Science Foundation, under Grant No. DMR-86-10837.

APPENDIX

The calculated line shapes in Figs. 3 and 6 were determined by the sum of three functions of the kinetic energy, x. An exponential function was used to match the background intensity, the Fermi function was used for the Fermi level, and asymmetric Gaussian function(s) represented the spectral features. Asymmetric peaks were necessary to model the interaction between the photoelectron and the valence electrons. Parameters for the exponential function,

$$E(x)=A\exp(Bx)\ , \tag{A1}$$

were obtained from a least-squares fit to experimental intensities outside the area of interest, between 6 and 9 eV below E_F, and at E_F. In the Fermi function

$$F(x)=\frac{1}{\exp[(x-E_F)/k_BT]+1} \tag{A2}$$

(where E_F is the kinetic energy of the Fermi level, k_B is the Boltzmann constant, and T is the temperature), an artificial temperature was used to fit the Fermi-level cutoff to the experimental width. The asymmetric Gaussian peak function for a peak (i), $A_i(x)$, was produced by multiplying the low-energy side of the Gaussian function, $G(x)$, with an exponential tail function,

$$\begin{aligned} &A_i(x)=G(x) \quad \text{for } x\geq x_{0i}\ , \\ &A_i(x)=G(x)+[G(x_{0i})-G(x)]\exp(x-x_{0i})\delta \\ &\qquad\qquad\qquad\qquad \text{for } x\leq x_{0i}\ , \end{aligned} \tag{A3}$$

where $G(x_{0i})$ is the intensity of the Gaussian function for the peak (i) at the peak center, (x_{0i}). The final form of these functions,

$$L(x)=\left[E(x)+\sum_i A_i(x)\right]F(x)\ , \tag{A4}$$

provides sufficient flexibility and accuracy to calculate a line shape as a function of energy, x. The final peak positions, x_{0i}, and intensities, $G(x_{0i})$, were determined by minimizing an averaged least-squares function,

$$M=[L(x)-R(x)]^2/N\ , \tag{A5}$$

where $R(x)$ is the intensity of the experimental data point at an energy (x) and N is the number of data points in the energy range that is being analyzed. The results of this numerical analysis, shown by the solid lines in Figs. 3 and 6, accurately fitted the photoemission spectra.

[1]T. C. Hsieh, T. Miller, and T.-C. Chiang, Phys. Rev. Lett. **55**, 2483 (1985).
[2]J. G. Tobin, S. W. Robey, L. E. Klebanoff, and D. A. Shirley, Phys. Rev. B **28**, 6169 (1983).
[3]M. F. Onellion, C. L. Fu, M. A. Thompson, and J. L. Erskine, Phys. Rev. B **33**, 7322 (1986).
[4]J. E. Houston, C. H. F. Peden, P. J. Feibelman, and D. R. Hamann, Phys. Rev. Lett. **56**, 375 (1986).
[5]D. G. O'Neill and J. H. Weaver, Phys. Rev. B **35**, 5892 (1987).
[6]C. L. Fu and A. J. Freeman, Phys. Rev. B **35**, 925 (1987).

[7]L. E. Klebanoff, R. H. Victora, L. M. Falicov, and D. A. Shirley, Phys. Rev. B **32**, 1997 (1985).
[8]W. Drube and F. J. Himpsel, Phys. Rev. B **35**, 4131 (1987).
[9]B. T. Jonker, K.-H. Walker, E. Kisker, and G. A. Prinz, Phys. Rev. Lett. **57**, 142 (1986).
[10]C. L. Fu, A. J. Freeman, and T. Oguchi, Phys. Rev. Lett. **54**, 2700 (1985).
[11]R. Richter, J. G. Gay, and John R. Smith, Phys. Rev. Lett. **54**, 2704 (1985).
[12]J. G. Gay and R. Richter, Phys. Rev. Lett. **56**, 2728 (1986).
[13]C. Rau, C. Liu, A. Schmalzbauer, and G. Xing, Phys. Rev. Lett. **57**, 2311 (1986); C. Rau and S. Eichner, *ibid.* **47**, 939 (1981).
[14]L. E. Klebanoff, S. W. Robey, G. Liu, and D. A. Shirley, Phys. Rev. B **30**, 1048 (1984).
[15]S. A. Chambers, T. R. Greenlee, C. P. Smith, and J. H. Weaver, Phys. Rev. B **32**, 4245 (1985); S. A. Chambers, S. B. Anderson, and J. H. Weaver, *ibid.* **32**, 5149 (1985); S. A. Chambers, H. W. Chen, I. M. Vitomirov, S. B. Anderson, and J. H. Weaver, *ibid.* **33**, 8810 (1986); **35**, 2592 (1987).
[16]D. G. O'Neill, J. J. Joyce, T. W. Capehart, and J. H. Weaver, J. Vac. Sci. Technol. A **3**, 1639 (1985).
[17]R. G. Jordan, W. Drube, D. Straub, and F. J. Himpsel, Phys. Rev. B **33**, 5280 (1986).
[18]G. Zajac, S. D. Bader, and R. J. Friddle, Phys. Rev. B **31**, 4947 (1985).
[19]The experimental geometries used in this experiment allowed full use of symmetry selection rules. For a discussion of selection rules and ARPES techniques, see E. W. Plummer and W. Eberhardt, Adv. Chem. Phys. **49**, 553 (1982), and references therein.
[20]A region of degeneracy is inevitable since the bulk Au Γ_{12}- or $d_{x^2-y^2}$-derived band is relatively narrow with binding energies between 1.8 and 3.2 eV [see H. Eckardt, L. Fritche, and J. Noffke, J. Phys. F **14**, 97 (1984)] and the Cr Γ_{12}-derived bands are much wider with energies between 4.5 eV and E_F (see Ref. 27).
[21]Michael Tinkham, *Group Theory and Quantum Mechanics* (McGraw-Hill, New York, 1964).
[22]C. L. Fu and A. J. Freeman (private communication).
[23]S. Ohnishi, A. J. Freeman, and E. Wimmer, Phys. Rev. B **29**, 5267 (1984).
[24]G. Gewinner, J. C. Peruchetti, A. Jaegle, and R. Pinchaux, Phys. Rev. B **27**, 3 (1983).
[25]Setsuro Asano and Jiro Yamashita, J. Phys. Soc. Jpn. **23**, 714 (1967).
[26]The electronic structure for the AFM structure can be obtained by mapping the bcc bands into the smaller simple-cubic Brillouin zone with an appropriate change of the symmetry labels, as discussed in Ref. 27.
[27]J. L. Fry, N. E. Brener, J. L. Thompson, and P. H. Dickinson, Phys. Rev. B **21**, 384 (1980).

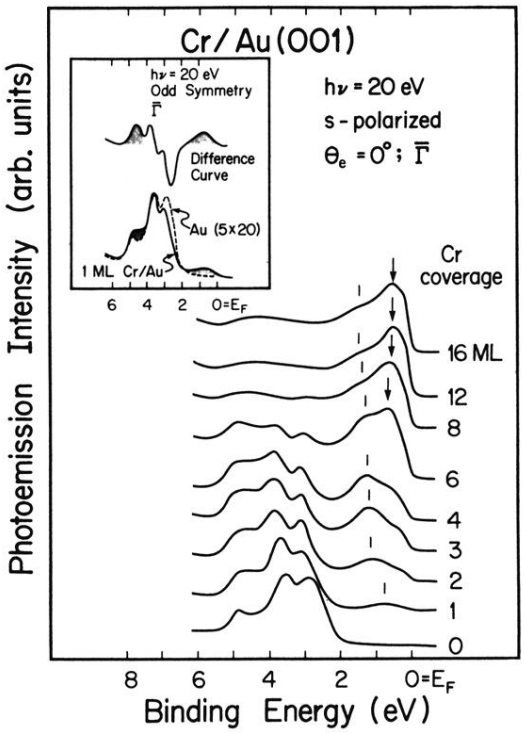

FIG. 1. Normal-emission spectra for Cr coverages from 0 to 16 ML Cr. The vertical bars highlight the evolution of the Δ_5 or $d_{xz,yz}$-derived bulk Cr band and the arrow points to the Cr $\bar{\Gamma}_5$ surface state which appears at 6 ML Cr coverage. The inset compares the spectra for clean Au(001) with 1 ML Cr/Au(001). Shading highlights the Cr-induced increases in intensity.